

Chapter 4

Nanoporous Materials and Confined Liquids

Petra E. de Jongh and Tamara M. Eggenhuisen

Abstract Nanoporous materials comprise zeolites, metal organic frameworks, disordered mesoporous oxides, ordered mesoporous oxides and carbon nanostructures. This chapter addresses the synthesis, structure and functional properties of each of these groups. Moreover, the changes in the physical properties of liquids confined in nanoporous materials are discussed. The altered properties of confined phases also form the basis for two important techniques to characterize nanoporous materials: physisorption and thermoporometry.

4.1 Introduction

Nanoporous materials contain pores with diameters up to 100 nm. Porosity is typically characterized by the specific pore volume (in cm^3/g) or porosity (in vol%), and the pore size distribution. As we will discuss below, the pore wall surface properties and specific surface area (in m^2/g) are also relevant parameters. Following IUPAC nomenclature, nanoporous materials are divided into three classes according to their dominant pore size range: *microporous* (up to 2 nm pores), *mesoporous* (2–50 nm pores) and *macroporous* materials (pores larger than 50 nm). This division is not always straightforward, as a single material can contain pores of different sizes (hierarchical porosity), and sometimes broad pore size distributions are found. Another important distinction is between *ordered and disordered porosity*. Ordered porous materials have a well-defined pore size, shape, and orientation. These materials are of great relevance for fundamental scientific research. Disordered materials have a random pore orientation, and generally wide pore size distributions. They are much easier to produce at low cost,

P.E. de Jongh (✉) · T.M. Eggenhuisen
Inorganic Chemistry and Catalysis, Debye Institute for Nanomaterials Science,
Utrecht University, Utrecht, The Netherlands
e-mail: p.e.dejongh@uu.nl

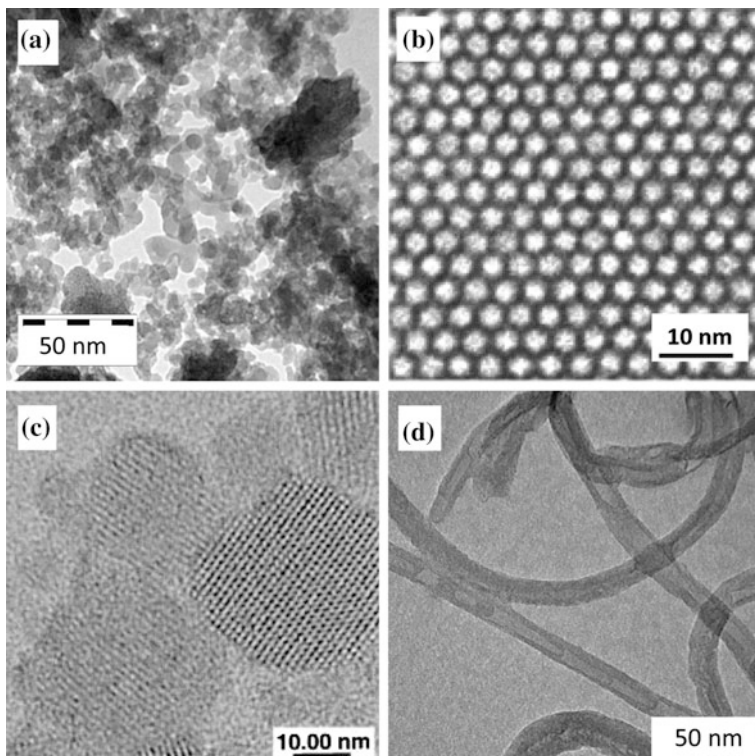


Fig. 4.1 Transmission electron micrographs illustrating the micro-structure of **a** disordered silica gel, adapted with permission from Ref. [1]; **b** ordered mesoporous silica (SBA-15), adapted with permission from Ref. [1]; **c** nanocrystals of microporous zeolite, reprinted from Ref. [2] with permission from the American Association for the Advancement of Science; and **d** an assembly of single walled carbon nanotubes. Note the different scale bars

and hence more relevant for practical applications. A few examples of porous materials are shown in Fig. 4.1.

Micropores have dimensions of the order of that of small molecules. Zeolites (crystalline aluminosilicates) form a prominent class of microporous materials. They can act as size-selective sieves or sorbents for small molecules. Most common mesoporous materials are ordered or disordered metal oxides, but also mesoporous carbons, nitrides, carbides, and metals are known. The mesopore range is the most interesting pore size range to study fundamental size and confinement effects. Mesopores allow the incorporation of nanoparticles, bulky organic molecules, biological species, and enzymes. Macroporous materials generally are not size-selective; their pores allow easy diffusion of even large molecules. They can be interesting for optical applications, but are also widely used as support or sorbent. In the second subsection of this chapter we will treat four main classes of nanoporous materials: zeolites, molecular microporous materials, ordered and disordered mesoporous oxidic materials, and nanostructured carbon materials.

Liquids may be confined in the pores of nanoporous materials, which significantly changes the physical properties of the liquid, such as the boiling and freezing points. Wetting and capillarity are key concepts to understand these changes, and will be discussed in detail in Sect. 4.3.

4.2 Classes of Nanoporous Materials

4.2.1 Zeolites

Zeolites are crystalline microporous aluminosilicates with pore sizes up to 1.5 nm. The term “zeolite” was first used by a Swedish mineralogist called Cronstedt in 1756, and is derived from the Greek words “ζεω” (to boil) and “λιθος” (stone). It refers to the large amount of water released upon heating zeolites. The water is present in the pores at ambient conditions due to the small pore size and high hydrophilicity. Zeolites can be mined in volcanic regions, but have also increasingly been produced synthetically since the 1940–1950s. Nowadays almost 200 zeolite structures are known. Detailed information about zeolite structures and properties can be found at the authoritative website of the International Zeolite Association (IZA) [3]. Zeolite structures are identified by 3-letter codes, which are abbreviations of their full name. The structures of sodalite (SOD), faujasite (FAU, also called “zeolite Y”) and mordenite (MOR) are shown in Fig. 4.2. New zeolite structures are still being discovered and accepted by the IZA Structure Commission after proof of synthesis details and structural characterisation. Although most structures are based on Si frameworks containing Al, a few all-silica as well as differently composed zeolitic structures are known, for instance alumina-phosphates (ALPO’s) with Al^{3+} and P^{5+} alternating in the lattice. Zeolites find many applications: on a scale of several million tons/year in detergents, as selective sorbents in the food and pharmaceutical industry, agriculture, as ion-exchangers, and as catalysts and catalyst supports.

Zeolites are synthesized hydrothermally from precursors such as amorphous aluminosilicates or metal organic molecules [4]. Porosity is induced by the presence of templates (for instance alkyl ammonium ions, small molecules or ion pairs) during the crystal growth. The formation of zeolites takes place in three stages, similar to those observed in the formation of colloidal nanoparticles (see Sect. 6.3.3, Chap. 6 for details). In the *induction stage* the solution is equilibrated at lower temperature. *Nucleation* is critical: for a synthesis solution with a given composition often several different zeolite structures can be grown depending on experimental conditions (kinetic control). Therefore, meticulous control over the synthesis conditions is required and the solution should be very homogeneous in pH, concentrations, and temperature. Often seeds are used to steer the nucleation process. *Crystal growth* is slow, and generally takes several hours up to days even at the typical hydrothermal conditions (100–150 °C, autogeneous steam pressure).

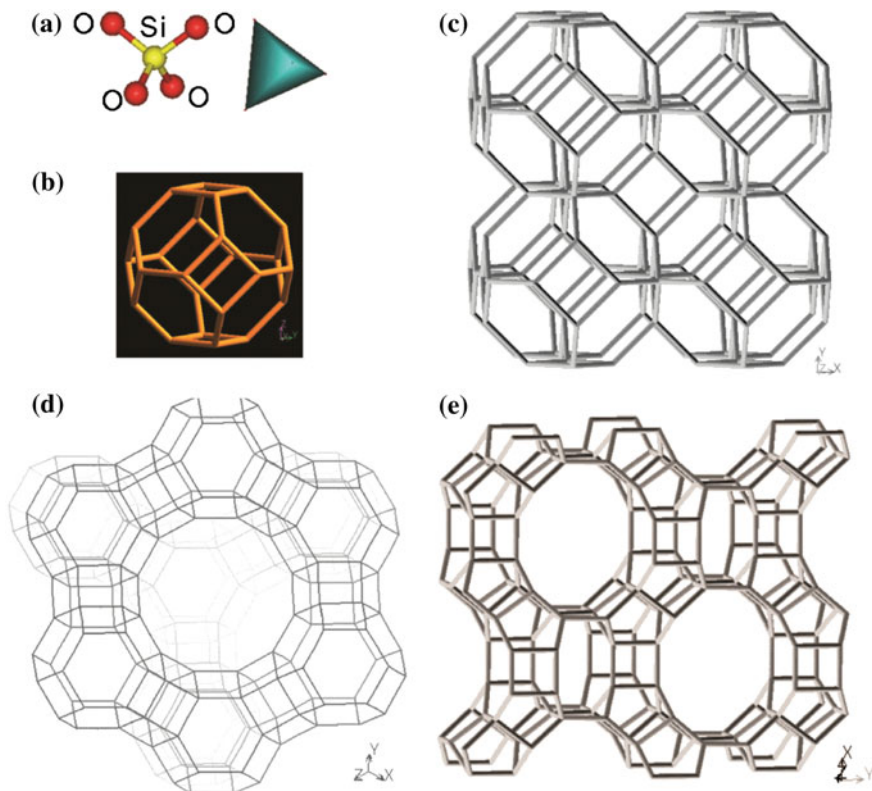


Fig. 4.2 TO_4 unit (a) is the primary building block that is used to construct larger composite building units such as the sodalite cage (b). These units can be arranged in different crystalline structures: (c) sodalite (SOD), (d) faujasite (FAU) and (e) mordenite (MOR). The structural models are not space filling: lines connect the metal cations in the structure, the oxygen anions are not represented. Images adapted with permission from Ref. [3]

After cooling, washing and filtering, the template is usually removed from the pores of the zeolite by heat treatment under air or inert atmosphere.

The primary building block of the zeolite structure is the TO_4 unit, a tetrahedron consisting of a central metal cation (usually Si^{4+}) and four (much larger) oxygen anions. The tetrahedra can be connected in different ways to form a 3-dimensional structure by sharing corners, edges or planes. Figure 4.2a schematically illustrates how different zeolitic structures can be assembled. By combining primary building blocks, secondary building blocks can be constructed, such as flat 4- or 6-rings. These can then be further assembled in larger composite building units, such as the sodalite cage (Fig. 4.2b), which consists of 4 flat 6-rings of tetrahedra (or alternatively 6 flat 4-rings). Arrangement of these larger units into the crystalline zeolite structure determines the porosity of the zeolite, comprising cages, cavities and/or

channels. Sodalite (Fig. 4.2c) and faujasite (Fig. 4.2d) structures are both based on sodalite cages, but have different porosities. In Fig. 4.2e we see mordenite, another common zeolite, which is constructed out of 5-1 building blocks (a five-ring of tetrahedra with one extra tetrahedron connected).

An important parameter is the *size* of the pores, cages or cavities in the structure, which can be derived from the number of tetrahedra forming them. Another important characteristic is the *dimensionality of the porosity*: in how many dimensions can a small molecule (about 0.3 nm wide) cross the zeolite through the pores. The sodalite cage has an inner diameter of 0.63 nm, which is large enough to host an organic molecule. However the 6-ring entrances only offer an opening of 0.25 nm; no molecule larger than water can travel through sodalite hence sodalite has zero-dimensional porosity. In contrast, the sodalite cages in faujasite are arranged such that larger cavities and windows are created. The cages can host species up to 1.12 nm, while the windows are 0.74 nm. Faujasite, like most other zeolites, has a 3-dimensional porosity. Mordenite has parallel channels of about 0.65 nm, and hence one-dimensional porosity.

A last important feature that describes a zeolite structure is the *symmetry* of the porosity, which is also relevant for metal organic frameworks and ordered mesoporous materials. Like the symmetry of a crystal lattice, the symmetry of an ordered nanoporous material provides information about the spatial arrangement of the pores. It is based on the smallest unit cell that can be used (by translation) to describe the entire 3D pore structure (space filling). For sodalite (Fig. 4.2c) the centres of 8 sodalite cages form the corners of the cubic unit cell. The full symmetry (space group) of each structure is denoted by 4 symbols, which give the symmetry elements that can be found in the unit cell. As an example: sodalite is designated “*Im $\bar{3}m$* ”, which means that its cubic unit cell has inversion symmetry (“*I*”) as well as mirror planes (“*m*”) and a three-fold rotation axis along the body diagonal (“*3*”). Identification of pore symmetries is based on X-ray crystallographic data, and in recent years has been supplemented by advanced electron microscopy methods.

The exact chemical composition of zeolites can vary, a property that is the basis for two major applications. Though the structure is based on SiO_2 , the Si^{4+} ions can be replaced by other metal cations that are small enough to favor tetrahedral coordination. Most common is replacement of part of the Si^{4+} ions by Al^{3+} ions. This leaves a net negative charge on the framework, which is compensated by cations present inside the pores, typically protons or small alkaline or alkali earth ions such as Na^+ or Li^+ . These cations are easily exchanged by other cations. For instance when zeolites are applied as “softener” in detergents, they exchange the Ca^{2+} or Mg^{2+} cations in “hard” water for cations that lead to more soluble salts (e.g., Na^+). Another major industrial application of zeolites is as acid catalyst for instance for (hydro)cracking and isomerisation reactions, in which intrapore protons provide acid catalytic sites.

4.2.2 Metal-Organic and Organic Microporous Materials

Zeolites are found in nature and have been known for centuries. In contrast, metal-organic frameworks (MOF) form a relatively new class of materials, which can only be obtained synthetically [5, 6]. Like zeolites, MOF are ordered microporous crystalline materials but they consist of metal ion complexes (“nodes”) that are connected by organic bridging ligands (“linkers”). Although polymeric porous materials had been known for some time, only in 1995 compounds containing dicarboxylate units were reported that were structurally stable upon removal of the solvent and thermal treatment.

Figure 4.3 shows the structure of MOF-5, one of the most studied MOF’s, which consists of $Zn_4O_6^+$ nodes and benzene-1,4-dicarboxylate linkers, forming a cubic lattice with cages of 1.2 nm that are accessible via 0.8 nm windows. The pore size, geometry and also the chemical and physical properties of MOF can be varied by choosing different linkers and nodes, and the theoretical number of structures that can be formed is enormous. 15 years after their discovery already more than 10,000 structures are known. One of the important structural differences with zeolites is that the primary building blocks are not limited to tetrahedra. A node can be connected to 2, 3, 4, 5, 6 or 8 linkers in different geometric configurations, while the linkers can bridge 2 nodes or more, allowing for an almost unlimited variety in structures.

The nodes in MOF are complexed metals (Zn, Cu, Co, Ni, Mg), while the linkers are organic ligands which often comprise N atoms. Some MOF can be synthesized hydrothermally, but solvothermal synthesis (growth in non-aqueous solution) is more common. Generally growth of the crystal is slow (in the course of days) starting from solutions containing metal precursor salts such as nitrates, and organic ligands. Additional templates can be used to induce porosity, but often the solvent molecules themselves act as template.

Post-synthesis modification is widely applied to induce functionality by covalently attaching extra groups to the organic ligands, or by incorporating nanoparticles or ions. MOF can be surprisingly stable upon solvent removal and further heating, but

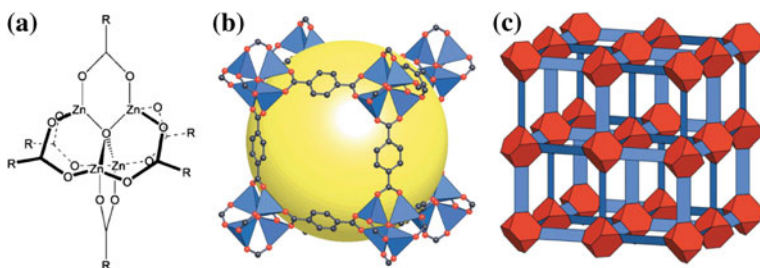


Fig. 4.3 a Structure of the Zn_4O_6 node and carboxylic linkers in MOF-5; b MOF-5 cage of 1.2 nm (indicated by the sphere) which is accessible via 0.8 nm windows; c MOF-5 has a cubic unit cell arrangement. Reprinted by permission from Macmillan Publishers Ltd: Nature, **423**, 705–714 (Ref. [6]), copyright (2003)

generally only in inert atmosphere (without water or oxygen). As they are composed of light elements, MOF can reach pore volumes as high as 2–3 cm³/g, and specific surface areas up to 3,000–6,000 m²/g. They are considered for a variety of applications in separation and reversible gas storage, as well as for catalytic, optical, and magnetic applications. The functionality is either inherent to the metal-organic framework, or due to guest species that are introduced into the cages. However, practical relevance still has to be proven. At present MOF are expensive, as most organic linkers are not commercially available. Also the limited stability and poor mechanical properties are a disadvantage for many applications.

In 2005 it was reported that also all-organic ordered nanoporous frameworks (Covalent Organic Frameworks, COF) could be synthesized [7]. An example is COF-1, which is based on diboronic acid units which are connected by a condensation reaction to form covalently bound planar and rigid sheets. These sheets self-assemble (bound by mostly van der Waals and also electronic interactions) into ordered 3-dimensional porous structures. Because COF are made of light elements, their porosity and specific surface area rival those of MOF (e.g. ~1 cm³/g and ~1,600 m²/g for COF-5). A porous network that is covalently bound in three dimensions can be formed when using building units with four connections such as tetra(4-di-hydroxyborylphenyl)methane (TBPM).

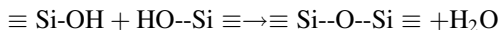
Shortly after the discovery of COF's another class of crystalline microporous solids was reported: zeolitic imidazolate frameworks (ZIF's). The stability of these materials is quite high compared to MOF. For instance, ZIF-8 and ZIF-11 are stable if boiled in alkaline solution, or heated up to temperatures of 550 °C. ZIF combine some of the properties of zeolites with those of MOF. They are based, like MOF, on metals (usually Zn, Co or Cu) and organic linkers. However, the organic linker is always an imidazolate unit, a conjugated 5-ring which contains 2 nitrogen atoms. The imidazolate unit binds to two transition metal atoms with a fixed bond angle very close to that of the Si–O–Si bonds in crystalline silica and zeolites (109°). As a result the framework structures, and hence pore symmetries, follow those of the zeolites. For instance ZIF-67 and ZIF-8 have the same framework and pore symmetry as the zeolite sodalite (*Im3 m*), but contain Zn (ZIF-67) or Co (ZIF-8) metal ions. By choosing different imidazolate linkers the pore or cage size can be tuned systematically. The number of ZIF is rapidly expanding, with close to 100 reported within the first 5 years after discovery.

4.2.3 *Disordered Mesoporous Metal Oxides*

Disordered metal oxides form a class of nanoporous materials that is widely used in industry. The nanoporosity of these materials is typically formed by interparticle spaces: primary particles of a few to a few tens of nanometres aggregate into μ -sized secondary particles. This results in an interparticle mesoporosity of 0.1–0.3 cm³/g. The porosity is not well-defined; it comprises different pore shapes and generally a wide pore size distribution. Therefore, these materials are of less

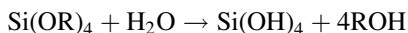
interest for fundamental studies than the ordered mesoporous materials that will be treated in the next Sect. 4.2.4. Two synthesis strategies are generally employed to prepare disordered metal oxide materials: solution (usually aqueous phase) synthesis or gas phase synthesis. Porous silica (used as filler material, desiccant, chromatography stationary phase, and catalyst support) is used as an example, but other porous metal oxides can be prepared in similar ways, and especially the solution-based route is also relevant for the ordered mesoporous oxides discussed below (Sect. 4.2.4).

A first preparation strategy is gelification from aqueous silicate solutions [8]. Natural sodium silicates can be dissolved in alkaline solution, forming a multitude of species such as $\text{Si}_2\text{O}_7^{6-}$, $\text{Si}_3\text{O}_{10}^{8-}$ and cyclic structures such as $\text{Si}_4\text{O}_{12}^{8-}$. Solubility in neutral and acid solution is low, hence acidification of the solution (for instance by adding H_2SO_4) or alternatively evaporation of the solvent, leads to the formation of a solid by condensation:



The condensation is governed by parameters such as temperature, concentration of the different species, and especially pH. At high pH the silicate species or hydroxyl surface groups of formed silica particles are deprotonated and hence negatively charged. As a result they repel each other. As the silicate solubility is also high, the dominating growth mechanism is Ostwald ripening by the preferential addition of monomeric silicates (which might originate from the dissolution of smaller particles) to larger particles, leading to spherical crystalline SiO_2 particles. At a low pH, close to the isoelectric point of silica (pH = 2–3), the species and particles are net uncharged. As condensation is slow and the growing species are not stabilized by electric repulsion, 3D aggregated networks with small pores are formed.

Very pure (and more expensive) porous silica can be obtained starting from metal-organic precursors, such as tetra-ethoxy-silane, $\text{Si}(\text{OC}_2\text{H}_5)_4$ (TEOS). In this case the condensation reaction is preceded by hydrolysis of the precursor:

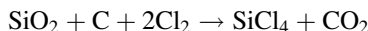


but still the final product is SiO_2 as the organic group is removed as an alcohol. This route also allows the formation of hybrid inorganic-organic materials with a lower degree of condensation, by introducing non-hydrolysable groups such as methyl-trimethoxy-silane in the precursor. The incorporation of organic groups leads to higher hydrophilicity and different mechanical properties (more flexibility) of the material.

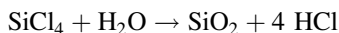
Nanoparticles can be observed once they have grown large enough to induce light scattering, while the formation of 3D networks becomes evident from a viscosity increase of the solution and gel formation upon prolonged reaction. It should be noted that the reaction can be stopped at the early stages allowing the preparation of free-standing allowing the preparation of colloidal silica nanoparticles as small as

10–20 nm as well as encapsulation of nanoparticles of other materials (e.g. gold or semiconductors) inside silica shells (see Chap. 6 for details). A very suitable technique to follow the progress of condensation is ^{29}Si NMR, which detects quantitatively the concentration of Si in different condensation states: e.g. Si(O) (not bound to any other Si atom via an oxygen), Si(I) (having formed one Si–O–Si bond), and fully condensed Si(IV) (forming the tetrahedral Si–O–Si coordination also found in quartz). After reaction the solid product is filtered and washed, and generally heated in inert atmosphere to further increase the degree of condensation in the materials. A wide range of metal oxides can be prepared via sol-gel chemistry in aqueous solutions. However most metal ions are more electropositive than silicon, leading to faster reaction and limited control over the particle morphology and hence porosity.

An alternative preparation route for metal oxide nanoparticles is via a gas phase reaction. A good example is the so-called Aerosil® process in which the starting material is a macroscopic silica such as sand. It is converted into the silica precursor by carbo-chlorination:



In a second step the gaseous silicon tetrachloride is converted into silicon dioxide at high temperatures (typically $\sim 1,000$ °C) by reaction with methane and oxygen, or alternatively with water (“flame hydrolysis”) which is formed in situ by co-feeding H_2 and O_2 :



The primary particle size (and hence the pore size in the resulting aggregates) is tuned by choosing the reaction conditions such as temperature, concentrations, and residence time in the flow through reactor. In addition to SiO_2 , TiO_2 , Al_2O_3 and ZrO_2 are also routinely prepared by flame hydrolysis.

For the production of nanoparticulate metal oxides it is important to realize that for many of them different polymorphs exists. Preparation of the final material generally involves heat treatment, and phase transitions can occur leading to a rearrangement of atoms and loss of the porosity that had been induced at room temperature. Typical examples are the anatase to rutile phase transition of TiO_2 , and the different polymorphs of Al_2O_3 sequentially formed upon heating.

4.2.4 Ordered Mesoporous Materials

In 1992 a new type of mesoporous material was reported that cannot be found in nature: ordered mesoporous silica. To prepare them, silica is grown in aqueous solution in the presence of surfactant molecules that have been added in such a high concentration that they form ordered micellar structures [9]. After filtering and

drying the template molecules are removed (combusted by heating in air, or leached out with, for instance, an acid). The imprint left by the micellar structure leads to 3D ordered mesoporosity in the silica. An important difference with zeolites (Sect. 4.2.1) is the size of the pores. Zeolites are microporous, having pores up to about 1.5 nm, while the pore sizes of ordered mesoporous silica are in the 1.5 to 50 nm range. Also, although the pore structure is ordered, the silica itself that forms the pore walls is amorphous, in contrast to zeolites which are crystalline. This limits the (hydro)thermal and mechanical stability of these materials.

Ordered mesoporous materials are commonly used for fundamental studies as their pore geometry and size are well defined and can be easily tuned by varying surfactant chain length, concentration, pH, temperature and solvent. Above the critical micelle concentration, surfactant molecules form isotropic micelles which upon further increase in concentration arrange into hexagonal, cubic or lamellar arrays. This provides a wealth of possible geometries, which can be “inverted” by using an apolar rather than a polar solvent to grow the metal oxides. Lamellar structures are generally not stable after surfactant removal.

The ordered mesoporous silica material MCM-41 is one of the earliest and most prominent examples. MCM-41 stands for “Mobil-Composition of Matter—No 41”, as Exxon Mobil was the first to report its synthesis in open literature [10]. As illustrated in Fig. 4.4, MCM-41 is templated by a cationic surfactant: cetyltrimmoniumbromide (CTAB, cetyl = hexadecyl). These template molecules form tubular micelles, resulting in parallel pores aligned in a hexagonal symmetry ($P6mm$). The pore size distribution is narrow and around 2 nm. The pore walls (~ 0.5 nm thick) are smooth and no intrawall porosity is present. Using the same surfactant molecules but different experimental conditions other structures can also be synthesized such as MCM-48 (a cubic structure) and MCM-50 (a lamellar structure).

In 1998 it was reported that also block-copolymers could be used as templates [11]. The first material synthesized was SBA-15. SBA stands for “Santa Barbara Acid”, as it was a group at this university that first reported the synthesis, which is

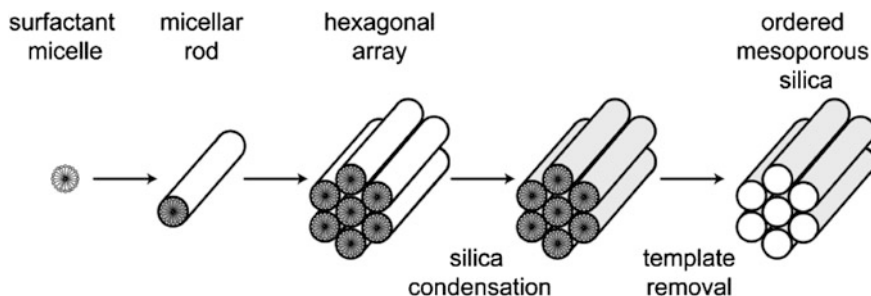


Fig. 4.4 The formation of ordered mesoporous silica (MCM-41): at high surfactant concentrations the micelles pack into rods, and the rods pack into regular hexagonal structures. Upon deposition of silica from the aqueous phase (which is excluded from the hydrophobic inner core of the micelles) a nanocomposite is formed. After removal of the micelles by heat treatment, a highly porous silica structure remains. Figure based on Ref. [10]

executed in acid solutions, rather than the alkaline conditions under which MCM type materials are grown. In the presence of a tri-block-copolymer, polyethylene-oxide-polypropyleneoxide-polyethyleneoxide (PEO₂₀-PPO₇₀-PEO₂₀) hexagonally ordered mesoporous silica with cylindrical pores was prepared. Key is the difference in hydrophilicity between PPO and PEO. Micelles form with a PPO hydrophobic core, while silica can grow in the aqueous phase that is intermixed with the more hydrophilic PEO units. After silica condensation, drying, and removal of the template, relatively large pores result, typically 5–10 nm. The former presence of the polyethyleneoxide chains is marked by micropores in the silica pore walls. The pore walls are typically 1.5–2 nm. Also, for SBA type materials the pore walls are corrugated (curved on a nm scale) and the ordering of the pores on the longer length scales is not rigid resulting in wormlike particles.

Ordered mesoporous silica is easy to prepare. Also other metal oxides can be prepared in a similar way, but generally less ordered mesoporosity is obtained. Nevertheless a range of ordered mesoporous oxides, such as Al₂O₃, TiO₂, MgO, Co₃O₄, TiO₂ has been reported by now. An alternative route to ordered mesoporous materials was first reported in 1999: nanocasting [12]. In this synthesis method an ordered mesoporous silica structure is used as a mold. Carbon replicas are prepared by filling the pores with a carbon precursor, such as sucrose or furfuryl alcohol. The negative carbon replica of the silica structure is obtained by polymerization and carbonization of the carbon source in the pores, followed by removal of the silica by leaching with an HF containing or alkaline solution. Alternatively vapor-phase deposition can be used for instance using N-containing carbon precursors, as well as other techniques such as electroless deposition or electrodeposition.

The invention of ordered mesoporous materials has been very important for fundamental studies on the properties of nanoporous materials, and gases, liquids and solids confined in the pores of these materials. The flexibility and control over the porosity of these materials is unprecedented. For instance the pore size can be varied from 1.5 to 30–50 nm. A wide variety of compounds has been prepared via the nanocasting method. Inorganic-organic hybrid materials can be grown by choosing partly non-hydrolysable precursors, mixed oxides can be formed by using mixed precursors and post-synthesis grafting allows tuning of the surface chemistry.

4.2.5 Nanostructured Carbon Materials

A range of nanostructured carbon materials exist with varying surface chemistries and porosity. The industrially most relevant are the “activated carbons”. These materials are produced from low-cost natural products, such as wood, olive pits, coconut shell, or bones by heating to high temperatures (800–1,500 °C) in an inert atmosphere. Usually an “activation” treatment follows where additional porosity is introduced by acid or KOH leaching, steam treatment, or both. Activated carbons have a high microporosity with slit-like pores, but typically also some additional meso- and macroporosity. The pore size distribution is broad and due to the natural

origin of the starting materials there is often a relatively high amount of contamination (for instance with metal oxides, carbonates or sulfates). The high specific surface areas up to 1,000–1,500 m²/g and facile manufacture of activated carbons makes them widely applied for instance as absorbents (such as in potable and waste water treatment, decoloration of food products and air purification), automotive emission abatement and industrial processes such as solvent vapor recovery. The wide pore size distribution and poor control over the physicochemical properties make these materials less interesting from a research point of view. Carbon materials with higher purity can be obtained from synthetic precursors. For instance “carbon black” is produced by burning hydrocarbons in a low oxygen concentration. Aggregates of spherical particles with a size of a few nanometers are formed, hence analogous to disordered mesoporous silica the porosity arises from the interparticle spaces.

For fundamental studies, well-defined nanostructured carbons are much more attractive. Since their discovery in the early 1990s carbon nanotubes have attracted much attention [13]. They consist of a graphitic sheet, rolled up into a cylindrical tube. Nanotubes can have a diameter between 2 and 200 nm, while the length can be in the order of micrometers. They can be semiconducting or metallic, and have extraordinary mechanical strength. A variety of nanostructured carbon materials based on graphitic sheets exists. Multiwalled carbon nanotubes consist of multiple concentric graphitic cylinders. Furthermore, in herringbone type and platelet-like carbon nanofibres the graphitic sheets are not oriented parallel to the tube axis, but rather inclined and perpendicular respectively. Buckyballs or fullerenes and graphene sheets also attract much attention due to their exceptional properties.

Carbon nanotubes and fibers are generally produced by vapor phase processes and can be grown from CH₄ or CO and H₂ using supported metal nanoparticles as growth catalysts. The metal catalysts are usually removed by acid leaching, but it is difficult to remove all contamination. More expensive methods are carbon arc discharge or laser ablation processes. Processing carbon nanomaterials is more cumbersome than oxides as carbon nanotubes cannot be dispersed in aqueous solutions or organic solvents, and generally rapid precipitation occurs forming nanoporous materials consisting of entangled networks or bundles of individual nanostructures. An important difference between all carbon materials and the metal oxides discussed earlier is the nature of their surface. Graphite is hydrophobic, and has a very low surface energy. As a consequence its interaction with gases, liquids and solids is weak. As we will see later (Sect. 4.3), this has important implications when trying to deposit a material, whether liquid or solid, inside the pores.

4.3 Liquids Confined in Nanopores

In this section we discuss liquids confined in nanopores, and how the confinement influences the physical properties of the liquid phase, and the liquid-gas and liquid-solid transitions. Figure 4.5 (solid lines) gives a schematic representation of a phase

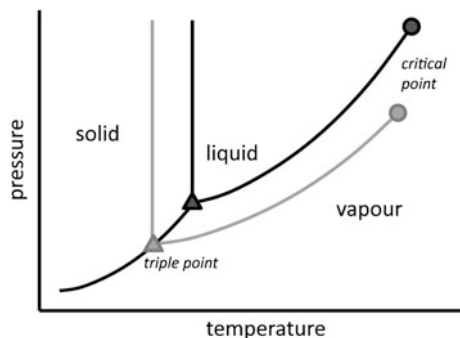


Fig. 4.5 Schematic phase diagram showing the solid, liquid and vapour phases as a function of temperature and pressure. *Solid line* a typical bulk material; *dotted line* confinement of the same material in nanopores leads to a depression of the melting point and an increase in the boiling point

diagram for a typical material with phase transitions from solid to liquid to the vapour phase occurring with increasing temperature or decreasing pressure. The triple point indicates the pressure and temperature at which solid, liquid and vapour phases co-exist. The critical point indicates the temperature and pressure above which liquid and vapour form a single continuous phase.

The dotted line indicates the changes in the phase diagram if the same material is confined in nanopores. Nanoconfinement generally results in a shift of the triple point to lower temperature and pressure. Concomitantly, the temperature for the solid-liquid equilibrium (melting/freezing point) decreases and the temperature of the liquid-vapor equilibrium (boiling/condensation point) increases. In rare cases due to a specific combination of matrix and liquid, a reverse shift can be observed. The origin of these effects lies in the interaction of confined liquids with the pore walls and will be discussed in more detail qualitatively and quantitatively in the following paragraphs, using the concepts of *wetting* and *capillary condensation*.

4.3.1 Wetting

Wetting is a crucial factor in determining not only the magnitude but also the sign/direction of changes in the physicochemical properties when confining a liquid in nanopores. An experimentally easily accessible measure for wetting is the contact angle θ . This is schematically illustrated in Fig. 4.6 which depicts a droplet of a liquid on top of a solid substrate. The terms γ_{sv} , γ_{lv} , and γ_{sl} denote the surface free energies of the solid and of the liquid, and the solid-liquid interfacial free energy, respectively. Please note that generally the term “*surface energy*” (given in J/m^2) is used for solids, while often “*surface tension*” (given in N/m) is used for liquids, although both units are interchangeable. All of these energies are fixed for a given combination of solid and liquid material (and gas atmosphere). The droplet will

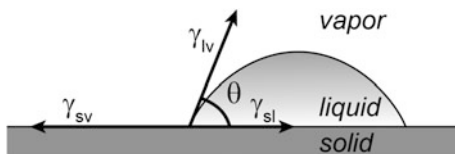


Fig. 4.6 Schematic illustration of a drop of liquid wetting a planar solid surface, with contact angle θ , and γ_{sv} , γ_{lv} , γ_{sl} being the interfacial energies [courtesy Rudy Wagemans]

adopt such a shape that the contact angle reflects the balance between the interfacial energies. As the contributions of the solid-vapour and liquid-solid interfacial energies exert forces parallel to the surface, it is easy to derive that in equilibrium the contact angle is defined by the Young equation:

$$\gamma_{sv} = \gamma_{sl} + \gamma_{lv} \cos \vartheta \quad (4.1)$$

Depending on the magnitude of the interfacial tensions, $\cos \theta$ can be either positive (i.e., $\theta < 90^\circ$) corresponding to wetting, or negative (i.e., $\theta > 90^\circ$) corresponding to dewetting. For instance water on a hydrophilic surface will easily wet: if a droplet is applied it will spread over the surface until in equilibrium the contact angle is far below 90° . On the contrary if the liquid is repelled by the surface, such as in the case of water on a hydrophobic surface, the droplet retracts, resulting in a final contact angle higher than 90° . Solids with polar surfaces, such as hydroxylated metal oxides, have high solid surface free energies, and are thus more easily wetted than solids with an apolar surface and hence low surface energy, such as graphitic materials. In general, apolar solvents (such as hexane, $\gamma_{lv} = 0.018$ N/m) have a lower surface tension and hence spread more easily on a given surface than polar liquids (e.g., water, having a surface tension of $\gamma_{lv} = 0.072$ N/m) or even molten metals (such as mercury, having a surface tension of $\gamma_{lv} = 0.5$ N/m).

We can now understand qualitatively that if the wetting of a solid surface with a liquid is favourable, confining this liquid into a nanoporous matrix of the solid material will enhance the stability of the liquid phase. Therefore, for wetting liquids confined in nanopores a decrease of the triple point will occur leading to a depression of the melting point and an increase of the boiling point. However, if a non-wetting situation occurs, the opposite is true, and the stability domain of the liquid phase becomes smaller as a result of the pore-confinement. The extent of these effects depends strongly on the pore size, and this is discussed in a more quantitative manner in the following sub-sections.

4.3.2 Capillarity and Capillary Condensation

At a fixed temperature the liquid-vapour equilibrium occurs at a pressure different than the standard condensation pressure p_0 if the interface between the two phases

is curved. The pressure difference Δp across an interface with an effective radius of curvature r_{eff} is described by the *Laplace equation*:

$$\Delta p = \frac{2\gamma_{\text{lv}}}{r_{\text{eff}}} \quad (4.2)$$

Δp is defined as the pressure difference between the liquid and the vapour phase, and the effective radius is positive for convex liquid surfaces and negative for concave surfaces. This means that for a convex liquid surface (e.g., a small liquid droplet in the gas phase) a positive value Δp is found. The pressure inside the droplet is larger than outside the droplet, and compensates the surface forces trying to further contract the droplet in order to minimise the surface area. For a concave surface (e.g., a gas bubble in a liquid) a negative pressure difference is found.

Filling nanopores with a liquid generally leads to curved liquid-vapour phase interfaces. In the simplest case, assuming cylindrical pores, a hemispherically shaped meniscus is present, for which the effective radius is determined by the pore radius r_p and wetting angle θ . Equation (4.2) can easily be modified to give the capillary pressure difference Δp across a liquid-vapour interface for a liquid confined in cylindrical pores with a radius r_p as described by the *Young-Laplace equation*:

$$\Delta p = \frac{2\gamma_{\text{lv}} \cdot \cos \theta}{r_p} = \frac{2}{r_p} (\gamma_{\text{sv}} - \gamma_{\text{sl}}) \quad (4.3)$$

We refer to the capillary pressure Δp as the pressure difference between the liquid and the vapour phase induced by the confinement in pores. If we assume perfect wetting ($\theta = 0^\circ$) and cylindrical pores, the Young-Laplace equation reduces to Eq. (4.2). The capillary pressure can be an important driving force to fill pores. An everyday example is the absorption of water into a sponge, and the mechanism that carries water up the microscopic tubes (xylem) inside a tree. Capillary pressure can be measured in capillaries by comparing the liquid level inside a capillary with that of the same liquid outside, as illustrated in Fig. 4.7. The capillary pressure causes a rise or fall in the liquid level which is balanced by gravity. In the case of, for instance, water in a glass capillary, a strong rise of the liquid level in the capillary results. On the contrary, if the capillary is placed in liquid mercury, the liquid level in the capillary will be significantly lower than that of the surrounding liquid.

An important consequence of the capillary pressure is that a liquid can condense in pores at vapour pressures much lower than the standard condensation pressure p_0 (compare in Fig. 4.5 the liquid-vapour transition pressure at a given temperature for the bulk and confined material). We refer to this phenomenon as **capillary condensation**. The condensation pressure for a perfectly wetting liquid is given by the *Kelvin equation*:

$$p = p_0 e^{-\frac{2\gamma_{\text{lv}}}{r_k T}} \quad (4.4)$$

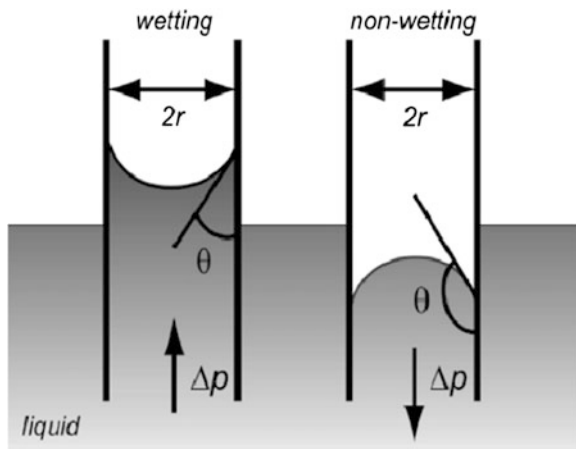


Fig. 4.7 Schematic illustration of the liquids levels in capillaries as a result of capillary pressure, illustrating the wetting case (*left frame*) for instance occurring for water in a glass capillary, as well as the dewetting case (*right frame*) which occurs for liquid mercury in glass [courtesy Rudy Wagemans]

in which v_1 denotes the molar volume of the liquid. The Kelvin equation is directly derived from the Laplace equation (Eq. 4.2) assuming ideal gas behaviour and a liquid molar volume that is independent of pressure. As expected, a high surface tension of the liquid will lead to a large deviation from the standard condensation pressure. Also, the smaller the pores, the larger the effect.

As an example, condensation of water vapour at 100 °C in pores of 1 μm occurs at a pressure very close to the standard condensation pressure ($p/p_0 = 0.9999$). However, in nanopores, water already condenses at significantly lower pressures: $p/p_0 = 0.998$ for 100 nm radius pores, $p/p_0 = 0.981$ for 10 nm pores, and only $p/p_0 = 0.826$ for 1 nm pores. The Kelvin equation can easily be modified to take non-ideal wetting into account by adding the term $\cos\theta$. However, most often this is not needed if we are studying liquid-vapour equilibria. The interaction of gas molecules with solid surfaces is generally strong enough to allow adsorption of a monolayer of molecules or atoms at pressures much lower than the condensation pressure. As a result, vapour typically condenses onto an internal pore surface which is already covered by a monolayer of the corresponding liquid, leading to low effective contact angles.

It is good to realize that the Kelvin equation is based on a macroscopic approach and hence inevitably breaks down for pores in the lower size range. For instance, it is not reasonable in this case to assume that the shape of the meniscus (which now consists of a limited number of molecules or atoms) is exactly hemispherical, or that the surface tension of such a highly confined liquid is the same as that for a bulk liquid. Nevertheless the Kelvin equation gives a very reasonable quantitative approximation of the impact of pore confinement on the liquid-gas equilibrium, and the shift in pressure (or, equivalently, in condensation temperature) associated with it.

4.3.3 Gas Physisorption

The influence of pore size on capillary pressure is the basis for the most common method of porosity determination: nitrogen physisorption [14]. It measures the equilibrium amount of adsorbed N_2 in a sample at liquid nitrogen temperature ($-196\text{ }^\circ\text{C}$ or 77 K) as a function of the relative pressure. A typical measurement is started in vacuum. Then for every measurement point a known amount of nitrogen is dosed to the sample container, and after equilibration the pressure is measured. The expected pressure for the given free volume if there would be no interaction at all between the nitrogen vapour and the solid is known. The difference between this reference value and the experimentally measured pressure directly yields the amount of nitrogen that is adsorbed by the sample. Measurement points are taken at increasing relative pressures up to the condensation pressure p_0 (1 bar for N_2 at $-196\text{ }^\circ\text{C}$). Subsequently, the desorption isotherm is recorded by stepwise decreasing the vapour pressure/amount of nitrogen in the system and recording the equilibrium pressures.

Physisorption gives a wealth of information about the porosity of the material. An example of a measurement is given in Fig. 4.8 for ordered mesoporous silica (MCM-41). The left frame shows the equilibrium amount of nitrogen adsorbed as a function of the relative pressure. As wetting is favourable, at low relative pressures gas molecules start adsorbing at the large SiO_2 surface, leading to a gradually increasing amount of adsorbate with pressure. From this part of the measurement the specific surface area (m^2/g) can be derived, which is dominated by the internal surface area of the nanopores. At a certain pressure, given by the Kelvin equation (Eq. 4.4), capillary condensation takes place, and liquid nitrogen suddenly condenses inside the nanopores leading to a steep increase in adsorption at a relative pressure of ~ 0.3 bar. This proves that a significant amount of mesoporosity is present. The specific

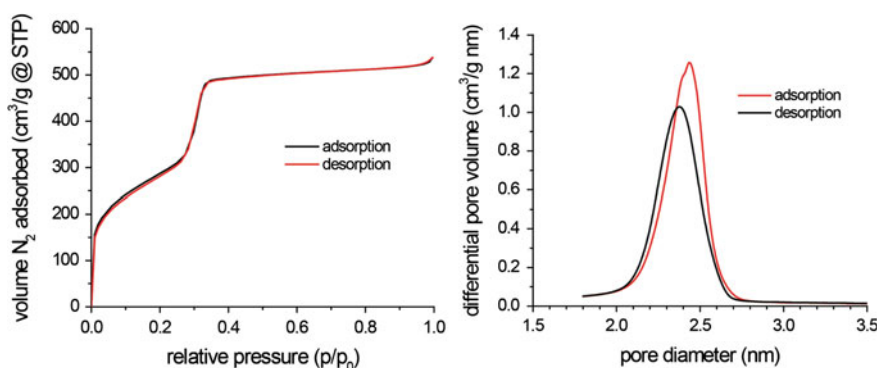


Fig. 4.8 N_2 physisorption isotherm measured at $-196\text{ }^\circ\text{C}$ for MCM-41. (left) Experimental N_2 uptake (expressed as the volume that the gas would have at standard T and p). (right) Pore size distribution derived from this measurement

mesopore volume is directly derived from the amount of nitrogen condensed in the pores. The pore size and pore size distribution (Fig. 4.8, right frame) are obtained by analysing this step in detail and using the Kelvin equation. Upon further increasing the pressure the adsorbed amount does not change much, as only some nitrogen adsorbs on the (small) external surface area of the particles. The shape of the physisorption isotherm, and specifically the hysteresis that is often observed (difference between adsorption and desorption branches of the physisorption isotherm) also contains information on pore shape and connectivity.

4.3.4 Changes in Melting Behaviour

Not only the liquid-vapour, but also the solid-liquid phase transition is affected by pore-confinement [15]. The melting point depression, ΔT , is inversely related to the effective radius of curvature r_{eff} , as described by the **Gibbs-Thomson equation** for a cylindrical pore (note that Thomson is Lord Kelvins given name):

$$\Delta T = T_0 - T_m(r_{\text{eff}}) = \frac{2T_0(\gamma_{\text{ws}} - \gamma_{\text{wl}})v_l}{\Delta H_m r_{\text{eff}}} \quad (4.5)$$

where T_0 is the bulk melting temperature, ΔH_m is the melting enthalpy and γ_{ws} and γ_{wl} are the pore wall-solid and pore wall-liquid interface energies. For a perfectly wetting liquid $\gamma_{\text{ws}} - \gamma_{\text{wl}} = \gamma_{\text{sl}}$. In this case the solid-liquid transition shifts to lower temperatures, and the Gibbs-Thomson equation can be simplified to:

$$\Delta T = \frac{C_{\text{GT}}}{r_p - t} \quad (4.6)$$

with C_{GT} a constant, and t the thickness of a non-freezing layer.

The surface tension, melting enthalpy and liquid molar volume are considered to be independent of the temperature. Even though this is a simplification (it is known that, for instance, the melting enthalpy of water decreases with decreasing temperature), it gives a reasonably good description of experimental results. Also, a non-freezing layer with thickness t is taken into account. Indeed, for water the existence of a non-ordered layer of molecules between the pore wall and ice core has been demonstrated, but there is no consensus on its thickness, as values between 0.20 and 1.05 nm are reported.

4.3.5 Thermoporometry

The influence of the pore size on the melting temperature is the basis for a second important technique to obtain information about porosity: thermoporometry. The

advent of ordered mesoporous silica materials has facilitated precise determination of the melting point depression as a function of mesopore size. These phase transitions can be measured by *Nuclear Magnetic Resonance* (NMR) or alternatively by *Differential Scanning Calorimetry* (DSC). With DSC the difference between the heat flows to either an empty container or to a sample-filled container is measured as a function of temperature, thereby detecting phase transitions occurring in the sample. Figure 4.9 shows the experimental data for the melting of ice confined in a series of ordered mesoporous silica with pore radii spanning from 1.5 to 6.2 nm. It shows that water confined in an SBA-15 material with a pore radius of 4 nm melts at $-16\text{ }^{\circ}\text{C}$, while water confined in a MCM-41 silica with a pore radius of 2 nm has a melting point depression of $43\text{ }^{\circ}\text{C}$ (see gray dashed lines in Fig. 4.9).

Thermoporometry is classically performed using water as adsorptive, allowing determination of melting points with a precision of $\sim 0.04\text{ }^{\circ}\text{C}$. For water in silica mesopores a lower pore diameter limit of $\sim 2\text{ nm}$ has been observed, below which the formation of ice was no longer detectable. However, also other adsorptives can be used, depending on the range of pore diameters under study and the nature of the porous material. Confined organic liquids including cyclohexane, nitrobenzene and various aromatic molecules also show pore size dependent phase transition temperatures. For these molecules a larger melting point depression as a function of the pore radius as compared to water is observed, enhancing the resolution at larger pore diameters.

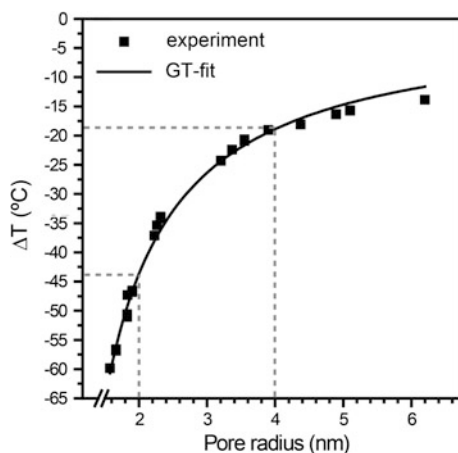


Fig. 4.9 Melting point depression as function of the pore radius. Symbols are experimental values for the melting point onset temperature of water confined in ordered mesoporous silica determined calorimetrically. The solid line represents best fit for the Gibbs-Thomson equation with $C_{GT} = 66.5\text{ }^{\circ}\text{C nm}$ and $t = 0.48\text{ nm}$

4.4 Outlook

Nanoporous solids are an important class of nanomaterials, with a wide variety in chemical composition (e.g., carbon or metal oxides), porosity (e.g., microporous or mesoporous) and properties. Although some materials, such as zeolites and activated carbons, have been known for centuries, the last few decades have seen remarkably the “invention” of new classes of materials that cannot be found in nature. Most of these materials, such as ordered mesoporous silica and metal organic frameworks, possess a very high structural order, which means that pore size, shape and orientation are well-defined. As a result, they give access to a fundamental exploration of the structure of nanoporous materials, and the impact of confining phases inside well-defined nanopores.

A first very important result of the availability of ordered nanoporous materials has been a significant progress in characterization techniques such as physisorption and thermoporometry. These techniques are based on intriguing fundamental changes when confining phases inside nanopores, such as changes in melting and boiling points of confined liquids, which are increasingly being investigated and understood. The availability of ordered porous materials has also greatly facilitated understanding the fundamentals of the preparation and functionality of supported nanoparticles, as will be treated in detail in Chap. 5.

Many ordered nanoporous materials have only recently been synthesized and described, hence it is difficult to predict what the future will bring. Though deemed very promising for a myriad of applications and functionalities, very few practical applications have actually been realised yet. Regarding fundamentals, many changes upon confining phases in nanopores are still not understood. Examples include changes in the solubility of salts in confined liquids, phase nucleation in confined solutions, and changes in crystallisation behaviour (for instance, why different crystal structures of ice are formed in confinement). Nanoporous materials will undoubtedly remain a very active research area in the years to come.

4.5 Exercises

1. An important advantage of ordered mesoporous materials is that their pore diameter can vary, allowing fundamental studies as a function of pore size. Suggest at least two strategies to tune the pore size of ordered mesoporous silica prepared by sol-gel synthesis in aqueous solutions.
2. (a) How high could a tree grow if it relies only on capillary pressure to transport water up to its leaves? Assume that the tree is composed of a single capillary tube with a diameter of 12 μm (a typical pore diameter for xylem). Start by calculating the force of gravity as a function of height, and then equalling it to the

attractive force due to the capillary force (interaction between water and pore wall). Assume perfect wetting ($\theta = 0^\circ$).

(b) What other mechanisms help trees to grow even taller?

(c) And in comparison: how high is water lifted against gravity in a nanoporous material with 2 nm pore diameter?

3. The IUPAC officially distinguishes 6 different classes of N_2 adsorption isotherms based on their shape [14]. Shown below (Fig. 4.10) are schematic representations of the adsorption profiles of these 6 classes (if only one line is shown, the adsorption and desorption branches of the isotherm exactly overlap). Class II is a typical non porous solid, which is wetted well by the N_2 (e.g., silica).
 - a. Which class would represent a material with the same structure that is not wetted by N_2 ?
 - b. Which isotherm would represent a zeolite?
 - c. And which isotherm MCM-41?
 - d. Can you guess which material could lead to an isotherm such as represented in VI?

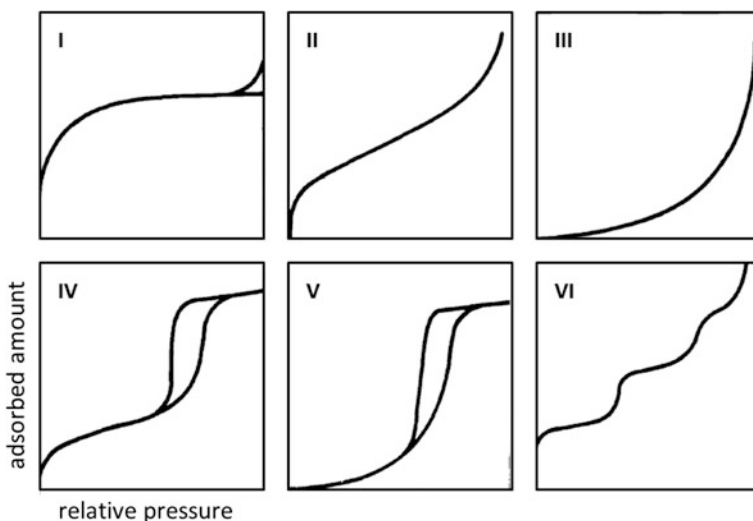


Fig. 4.10 Schematic representations of the 6 classes of N_2 adsorption isotherm profiles recognized by the IUPAC

References

1. Jong, K.P.: Support materials and characterization tools for nanostructured catalysts. *Oil & Gas Sci. Technol.* **61**, 527–534 (2006)
2. Mintova, S., Olson, N.H., Valtchev, V., Bein, T.: Mechanism of zeolite A nanocrystal growth from colloids at room temperature. *Science* **283**, 958–960 (1999)
3. Database of Zeolite Framework Types as provided by the Structure Commission of the International Zeolite Association (IZA-SC) which can be accessed via <http://www.iza-structure.org/databases/>
4. Cundy, C.S., Cox, P.A.: The hydrothermal synthesis of zeolites: History and development from the earliest days to the present time. *Chem. Rev.* **103**, 663–701 (2003)
5. James, S.L.: Metal-organic frameworks. *Chem. Soc. Rev.* **32**, 276–288 (2003)
6. Yaghi, O.M., O’Keefe, M., Ockwig, N.W., Chae, H.K., Eddaoudi, M., Kim, J.: Reticular synthesis and the design of new materials. *Nature* **423**, 705–714 (2003)
7. Côté, A.P., Benin, A.I., Ockwig, N.W., O’Keefe, M., Matzger, A.J., Yaghi, O.M.: Porous, crystalline, covalent organic frameworks. *Science* **310**, 1166–1170 (2005)
8. Brinker, C.J.; Scherer, G.W.: *Sol-Gel Science: the Physics and Chemistry of Sol-Gel Processing*. Academic Press, New York (1990)
9. Ciesla, U., Schüth, F.: Ordered mesoporous materials. *Microporous Mesoporous Mater.* **27**, 131–149 (1999)
10. Kresge, C.T., Leonowicz, M.E., Roth, W.J., Vartuli, J.C., Beck, J.S.: Ordered mesoporous molecular sieves synthesized by a liquid-crystal template. *Nature* **359**, 710–712 (1992)
11. Zhao, D., Feng, J., Huo, Q., Melosh, N., Fredrickson, G.H., Chmelka, B.F., Stucky, G.D.: Triblock copolymer synthesis of mesoporous silica with periodic 50 to 300 angstrom pores. *Science* **279**, 548–552 (1998)
12. Jun, S., Joo, S.H., Ryoo, R., Kruk, M., Jaroniec, M., Liu, Z., Shsun, T., Terasaki, O.: Synthesis of new, nanoporous carbon with hexagonally ordered mesostructure. *J. Am. Chem. Soc.* **122**, 10712–10713 (2000)
13. Baughman, R.H., Zakhidov, A.A., de Heer, W.A.: Carbon nanotubes: the route towards applications. *Science* **297**, 787–792 (2002)
14. Sing, K.S.W.: Reporting physisorption data for gas/solid systems. *Pure Appl. Chem.* **54**, 2201–2218 (1982)
15. Alba-Simionesco, C., Caosne, B., Dosseh, G., Dudziak, G., Gubbins, K.E., Radhakrishnan, R., Sliwiska-Bartowiak, M.: Effects of confinement of freezing and melting. *J. Phys. Condens. Matter* **18**, R15–R68 (2006)